Supporting Information

Human Recombinant Elastin-based Bioinks for 3D Bioprinting of Vascularized Soft Tissues

*Sohyung Lee, Ehsan Shirzaei Sani, Andrew R. Spencer, Yvonne Guan, Anthony S. Wiess, and Nasim Annabi**

Table of Contents:

Methods

Figures

Figure S4. MeTro/GelMA lattice constructs printed up to 16 layers to form constructs with a linear relationship between the number of layers and the height of the construct.

Figure S5. Post printing stability of 3D printed MeTro/GelMA constructs.

Figure S6. Degradation of 3D printed MeTro/GelMA constructs.

Figure S7. 2D cell seeding on 3D printed MeTro/GelMA constructs.

Figure S8. 3D bioprinting of 3T3 cells-laden MeTro/GelMA lattice.

Figure S9. 3D bioprinting of lattice scaffolds with HUVECs and CMs/CFs.

Figure S10. Rheological properties of GelMA bioink.

Figure S11. Optimizing printing conditions for GelMA bioink.

Figure S12. Degradation rate of lattice constructs printed with GelMA bioink at days 0.5, 1, 3, 7 and 14 post incubation in collagenase solution.

Figure S13. Representative images of 3D printing and photo-crosslinking of vascularized cardiac constructs.

Figure S14. 3D bioprinting and live/dead staining of vascularized cardiac constructs.

Figure S15. Evaluation of endothelium barrier function of 3D bioprinted constructs.

Figure S16. Evaluation of synchronized cardiac beating of 3D bioprinted constructs.

Figure S17. Representative H&E and IHC staining images of the subcutaneously implanted 3D printed and bioprinted cardiac constructs at day 14 post implantation.

Movies

Movie 1. Printing of vascularized cardiac construct at 8x speed. (red: parenchymal tissue, green: vessel)

Movie 2. Photocrosslinking of printed vascularized cardiac construct at 8x speed.

Movie 3. Beating of cardiomyocytes at day 5 post printing.

Movie 4. Beating of cardiomyocytes at day 10 post printing.

Movie 5. Beating of cardiomyocytes at day 15 post printing.

Methods

1. Synthesis of gelatin methacryloyl (GelMA)

GelMA was synthesized as previously described elsewhere.[1, 2] Briefly, 10 g gelatin derived from cold-water fish skin (Sigma-Aldrich) was dissolved in 100 ml Dulbecco's phosphate buffered saline (DPBS) and heated to 60 °C for 30 min. Next, 8 ml methacrylic anhydride (Sigma-Aldrich) was added gently and dropwise to the gelatin solution under vigorous stirring (300 rpm) at the same temperature. The reaction was stopped after 3 hours by adding 300 ml DPBS and dialyzed in dialysis tubing (Spectrum Laboratories, MWCO = 12-14 kDa) against deionized (DI) water at 50 °C for 5 days to remove any unreacted methacrylic anhydride. After sterile filtration, the solutions were subsequently lyophilized for 4 days to generate a fibrous white foam.

2. Synthesis of methacryloyl substituted tropoelastin (MeTro)

Tropoelastin was expressed in bacteria and purified essentially as described previously.[3] Methacrylated tropoelastin (MeTro) was synthesized as previously described elsewhere.[4] Briefly, 2 g tropoelastin (Synthetic Human Elastin without domain 26A, recombinant human tropoelastin isoform SHELdelta26A) was dissolved in 20 ml DPBS at 4 °C to reach a 10% (w/v) tropoelastin solution. Once completely dissolved, 3 ml methacrylic anhydride was added dropwise to the solution and allowed to homogenize at 4 °C. The reaction was stopped after 16 hours by adding 20 mL DPBS (pre-cooled at 4 °C) to the solution. This solution was then dialyzed against DI water at 4 °C in a dialysis cassette (Slide-A-Lyzer™, MWCO = 3.5 kDa) for 3 days. After dialysis, MeTro was lyophilized for 4 days.

3. Proton nuclear magnetic resonance (^{1}H NMR) characterization

Spectra were acquired with Bruker AV400 NMR spectrometer for uncrosslinked GelMA and MeTro dissolved in deuterated dimethyl sulfoxide (DMSO-d6) and the supernatant from a partially dissolved composite (50/50 GelMA/MeTro, 15% (w/v) total polymer concentration) kept under vigorous shaking in DMSO-d6 overnight at room temperature. The degree of methacryloyl groups consumption was calculated by the following equation, where PA_b is equal to the peak area before crosslinking, and PA_a is the peak area after crosslinking (n = 3):

$$\text{Degree of methacryloyl consumption}(\%) = \frac{(PA_b - PA_a)}{PA_b} \times 100\ \% \quad (1)$$

Peak areas were measured using TopSpin 3.5pl4 to integrate the area of the curve with respect to phenolic conjugated peaks at d = 6.5–7.5 ppm.

4. Mechanical characterization

Hydrogel samples were prepared in rectangular PDMS molds (12 mm length, 6 mm width, 1.5 mm height) for tensile test or in cylindrical molds (6 mm diameter, 3 mm height) for compression test as described before. The dimensions of the hydrogels were then measured using a caliper. An Instron 5542 mechanical tester was used to perform tensile and cyclic compression tests. For the tensile test, hydrogels were placed between two pieces of tape within tension grips and extended at 1 mm/min until failure. The tensile strain and stress placed on the hydrogel samples were recorded through the Bluehill 3 software during the test and the compressive moduli of the hydrogels were calculated from the slope of the stress-strain curves. For the compression tests, hydrogels were loaded between compression plates. Cyclic compression tests were performed at 50% strain level and a rate of 1 mm/min by performing 10 cycles of loading and unloading. The compressive strain and stress on the

samples were measured using the Bluehill 3 software and the compressive moduli were obtained from the linear region (0.15-0.25 mm/mm strain) in the stress-strain curve. Energy loss were determined based on the area between the loading and unloading curves for cycle 8. (n = 4)

$$\text{Energy Loss (\%)} = \frac{\text{Area below loading curve} - \text{Area below unloading curve}}{\text{Area below loading curve}} \times 100\ \% \quad (2)$$

5. Preparation of Carbopol support bath

The Carbopol gel was prepared as described earlier with some modification.[5] Briefly, 1.8% (w/v) of Carbopol ETD 2020 (Lubrizol) was dissolved in 50 mL of Dulbecco's modified eagle medium (DMEM, Gibco) and vortexed. 1.1 mL of 10 M NaOH was added to 50 mL Carbopol solution and followed by vortexing until it became a gel. Next, the Carbopol gel was centrifuged at 1000 × g for 1 hour until the gel became homogeneously dispersed. The Carbopol gel were manually stirred with spatula once or twice during the centrifugation to facilitate the mixing process. The homogeneous Carbopol gel was kept in a 4 °C fridge for storage.

6. Rheological characterization

A rheometer (MCR 92, Anton Paar) equipped with a parallel plate with a gap size of 1 mm and a diameter of 8 mm was used to characterize the rheological properties of different solutions including MeTro/GelMA pre-polymers, gelatin solution, MeTro/GelMA bioinks and GelMA bioinks. Different solutions were prepared as outlined before and pipetted onto the rheometer. Any excess solution was trimmed with a spatula before these measurements.

Viscosity of MeTro/GelMA pre-polymers, gelatin solution and MeTro/GelMA bioinks were measured as a function of temperature. Shear rate was constant at 50 s^{-1} and the temperature

was swept at the rate of 2 ºC min^{-1}. To demonstrate the shear thinning behavior of the MeTro/GelMA bioinks, viscosity was measured as a function of temperature under three different shear rates of 5, 50 and 500 s^{-1}.

In a temperature sweep test, the storage modulus and the loss modulus were recorded as a function of temperature under a constant shear rate of 50 s^{-1}.

For a shear rate sweep test, viscosity and shear stress of bioinks were measured while shear rate was swept from 0.1 to 1000 s^{-1}. During the test, temperature for the GelMA bioinks and the MeTro/GelMA bioinks were set at 20 °C and 8 °C respectively.

The actual shear force applied on cells during the bioprinting was measured indirectly. Briefly, time spent for 1 ml bioink extrusion, T, was recorded and put into the equation below, where $\dot{\gamma}$ is shear rate (s^{-1}); V is volume of the extruded bioink (1 ml); d is diameter of printing nozzle (0.34 mm); T is time of extrusion (second).:

$$\dot{\gamma} = \frac{8V}{\pi d^3 T} \quad (3)$$

Then, the shear stress on cells according to the calculated shear rate was obtained from shear stress-shear rate data.

7. 3D printing of bioinks

Acellular and cell-laden bioinks were prepared as outlined before and were loaded into a 3 mL syringe affixed to a 25-gauge blunt end needle. Support baths were prepared as described and poured into a container large enough to hold the structure to be 3D printed. The syringe was loaded onto an INKREDIBLE+ bioprinter printhead from Cellink® and MeTro/GelMA bioink was maintained at 10 ºC. Pressure was varied to change the flow rate (10-25 kPa) of the bioinks and printed into different structures with a layer height of 250 μm with custom G-code. The printed structures were then exposed to light (405 nm) to crosslink up to 3 min

depending on the shape and the size of the structures, carefully removed from the support bath with a spatula, washed with warm DPBS.

For 3D bioprinting, cells were mixed with the bioink before loading onto the bioprinter and the printed structures were further washed with media to facilitate the removal of Carbopol bath around constructs before they were immersed in media and kept in CO_2 incubators. The media was changed once in the first 30 min to remove unreacted photoinitiator, gelatin and remaining Carbopol gel and then changed every day.

8. *Enzymatic* degradation

MeTro/GelMA lattice (8 mm L × 8 mm W × 1 mm H) were printed as described previously. The printed constructs were incubated in DPBS at 37 °C in order to remove the residual gelatin and Carbopol in the printed constructs for 3 days. The DPBS solution was refreshed on a daily basis. The dry weights of the samples were measured after freeze-drying. The samples were immersed in 1 mL of DPBS containing 10 units/mL of collagenase II (Worthington Biochemical, Lakewood, NJ, USA) and incubated at 37 °C. Samples were removed from the collagenase solution, lyophilized and weighed at different time points (days 0.5, 1, 3, 7 and 14). The degradation rate was calculated following the equation, where W_d is the weight of dried samples after degradation and W_0 is the initial weight of dried samples before swelling (n = 4):

$$Degradation\ Rate\ (\%) = \frac{W_0 - W_d}{W_0} \quad (4)$$

9. Cell culture and isolation

Human umbilical vein endothelial cells (HUVECs) were obtained from Lonza and cultured in endothelial growth BulletKit (EGM-2, Lonza) at 37°C in a humidified atmosphere containing 5 % CO_2. The 6–12th passages of HUVECs were used in this study.

Neonatal ventricular rat cardiomyocytes and cardiac fibroblasts were isolated at the UCLA NRVM core facility using 2- to 4-days old rats. Myocytes and fibroblasts were separated using Percoll density gradient. NRVMs were used on the same day that they were provide and NRVFs were cultured under standard conditions (37 °C, 5% CO_2) in DMEM with 10% fetal bovine serum and 1% penicillin/streptomycin before they were used at passage 1-3.

10. Determination of cell viability

The viability of bioprinted neonatal cardiac cells and HUVECs was evaluated by LIVE/DEAD™ Viability/Cytotoxicity Kit (Invitrogen) at days 1, 3, 5, 7 and 15. Ethidium homodimer (EthD-1) and calcein AM were diluted into 50:1 and 200:1 with DPBS respectively. Depending on the structure, appropriate amount of the solution was assigned to 3D bioprinted constructs and incubated for 45 min in 5% CO_2 at 37 °C. Live and dead cells were observed by a fluorescence optical microscope (Primovert, Zeiss) or a confocal fluorescence microscope (SP8-STED, Leica). Living cells were detected by calcein AM (green fluorescence), and death cells by EthD-1 (red fluorescence). The number of viable cells was quantified using ImageJ (NIH) software. The number of cells was calculated by the ratio among the area of each cluster with the area of a known single cell. Then, the viability rate was obtained by comparing the number of viable cells with total number of viable and non-viable cells.

11. Immunofluorescence staining

Cell-laden structures were cultured under standard condition as described before. At different time points (days 5 and 10), samples were fixed for 1 h at room temperature using 4 % (v/v) paraformaldehyde (Sigma-Aldrich) in DPBS. Cells were permeabilized by soaking the samples in 0.1 % (v/v) Triton X-100 (Sigma-Aldrich) dissolved in DPBS for 30 min while

non-specific binding was inhibited using 10 % (v/v) bovine serum albumin (BSA, Sigma-Aldrich) for 1 h at room temperature. Samples were then incubated for overnight at 4 °C in a solution containing primary antibodies at 1:200 dilution in 10 % (v/v) BSA and 0.1 % (v/v) Triton X-100 in DPBS. In particular, rabbit polyclonal anti-CD31 (ab28364, Abcam) and mouse monoclonal anti-sarcomeric α-actinin (ab9465, Abcam) were used. Samples were then incubated for 1 hour at room temperature in a solution containing secondary antibodies at 1:400 dilution in 10 % (v/v) BSA in DPBS. Alexa 488-conjugated goat anti-mouse (ab150116, Abcam) and Alexa Fluor 594-conjugated goat anti-rabbit (a11008, Invitrogen) were acquired from Abcam and Invitrogen respectively. Nuclei of the cells were stained by 40,6-diamidino-2-phenylindole (DAPI, Invitrogen). Images were taken using a fluorescence optical microscope (Primovert, Zeiss) or a confocal fluorescence microscope (SP8-STED, Leica).

12. Evaluation of endothelium barrier function

To assess barrier function of the printed vasculature, diffusional permeability was quantified by perfusing culture media with 25 μg/mL FITC-conjugated 70-kDa dextran (FITC-Dex; Sigma product 46945) in the vascular channel at a rate of 1mL/min for 20 min. The diffusion of FITC-Dex was monitored using tile scan of a fluorescence microscope with 2.5× objective (Zeiss). Fluorescence images were captured before perfusion and every 4 min. Diffusional permeability of FITC-Dex is calculated by quantifying changes of fluorescence intensity over time using the following equation:

$$P_d = \frac{1}{I_1 - I_b} \cdot \left(\frac{I_2 - I_1}{t}\right) \cdot \frac{d}{4} \quad (5)$$

P_d is the diffusional permeability coefficient, I_1 is the average intensity at an initial time point, I_2 is an average intensity after time t (s), I_b is background intensity (before introducing FITC-Dex), and d is the channel diameter (cm). The measurements are performed on embedded

channels with and without endothelium (n = 3).

13. Evaluation of cardiomyocyte beating

The beating behavior of the engineered cardiac tissues were assessed as previously described [6]. Briefly, individual CM contractions within the engineered cardiac tissues were quantified with a custom MATLAB code to calculate beats per minute (BPM) and degree of coordination using video microscopy. Cardiac cells were recorded at 30 frames per second and raw video files were exported as AVIs and imported into MATLAB for analysis. Regions of interest (ROIs) were identified from the first frame of the video recording as objects between 75 μm^2 – 1000 μm^2 in size. The average BPM was calculated as the mean number of contractions for all ROIs in field of view (m > 20) multiplied by 60 and divided by the video length from a minimum of three samples per condition (n > 3). Timestamps for each contraction from the identified CMs were assigned a unique identification number to gather a quantification on the degree of coordinated contraction in the tissue models.

14. Dorsal subcutaneous implantation of hydrogels

All animals were handled in strict accordance with good animal practice as defined in the federal regulations set forth in the Animal Welfare Act (AWA), the 1996 Guide for the Care and Use of Laboratory Animals, PHS Policy for the Humane Care and Use of Laboratory Animals, as well as UCLA's policies, and procedures as set forth in the UCLA Animal Care and Use Training Manual. All animal work was approved by the UCLA Chancellor's Animal Research Committee (ARC # 2018-076-01B).

3D printed cardiac tissue constructs (7.2 mm L × 7.2 mm W × 3 mm H) were used for this study to evaluate biodegradation and inflammatory response of the MeTro/GelMA and GelMA bioinks. The 3D printed constructs were immersed in DPBS and incubated at 37 °C

for 7 days to stabilize before implantation. Male Wistar rats (200−250 g) were purchased from Charles River Laboratories (Wilmington, MA, USA). 3D printed constructs were prepared under sterile conditions and their initial wet weights were recorded. General anesthesia and analgesia were induced by inhalation of isoflurane (2.5% (v/v)), followed by subcutaneous meloxicam administration (5 $mg \cdot kg^{-1}$). Next, 1.2 mm subcutaneous pockets were made through the posterior dorsal skin. The 3D printed constructs were then implanted into the subcutaneous pockets. The acellular tissue constructs were inserted into the left pocket and the right pocket respectively. Afterwards, the wounds were thoroughly closed with 3-0 polypropylene sutures. The tissue constructs were harvested at weeks 1, 2 and 3 post-implantations.

15. Histological and immunohistochemical analysis

Histological and immunohistochemical analysis were performed on cryosections of the explanted hydrogel samples in order to characterize the inflammatory response elicited by the implanted material. After explantation, samples were fixed in 4% paraformaldehyde for 4 hours, followed by overnight incubation in 30% sucrose at 4 °C. Samples were then embedded in Optimal Cutting Temperature compound (OCT) and flash frozen in liquid nitrogen. Frozen samples were then sectioned using a Leica Biosystems CM1900 Cryostat. 15-µm cryosections were obtained and mounted in positively charged slides. The slides were then processed for hematoxylin and eosin staining (Sigma) according to instructions from the manufacturer. The stained samples were preserved with DPX mountant medium (Sigma).

Immunohistofluorescent staining was performed on mounted cryosections as previously reported.[7] Anti-CD3 (ab16669) and anti-CD68 (ab125212) (Abcam) were used as primary antibodies, and an Alexa Fluor 594-conjugated secondary antibody (Invitrogen) was used for detection. All sections were counterstained with DAPI (Invitrogen), and visualized on an

AxioObserver Z7 inverted microscope.

References

[1] E. S. Sani, A. Kheirkhah, D. Rana, Z. Sun, W. Foulsham, A. Sheikhi, A. Khademhosseini, R. Dana, N. Annabi, Science Advances **2019**, 5, eaav1281.
[2] E. S. Sani, R. P. Lara, Z. Aldawood, S. H. Bassir, D. Nguyen, A. Kantarci, G. Intini, N. J. M. Annabi, **2019**.
[3] C. Baldock, A. F. Oberhauser, L. Ma, D. Lammie, V. Siegler, S. M. Mithieux, Y. Tu, J. Y. H. Chow, F. Suleman, M. Malfois, Proceedings of the National Academy of Sciences **2011**, 108, 4322.
[4] N. Annabi, Y.-N. Zhang, A. Assmann, E. S. Sani, G. Cheng, A. D. Lassaletta, A. Vegh, B. Dehghani, G. U. Ruiz-Esparza, X. Wang, Science translational medicine **2017**, 9, eaai7466.
[5] A. Spencer, E. Shirzaei Sani, J. R. Soucy, C. C. Corbet, A. Primbetova, R. A. Koppes, N. Annabi, ACS applied materials & interfaces **2019**.
[6] J. R. Soucy, J. Askaryan, D. Diaz, A. N. Koppes, N. Annabi, R. Koppes, Replicating the Diversity of the Myocardium with Low-Cost 3D Models **2018**.
[7] N. Annabi, D. Rana, E. S. Sani, R. Portillo-Lara, J. L. Gifford, M. M. Fares, S. M. Mithieux, A. S. Weiss, Biomaterials **2017**, 139, 229.

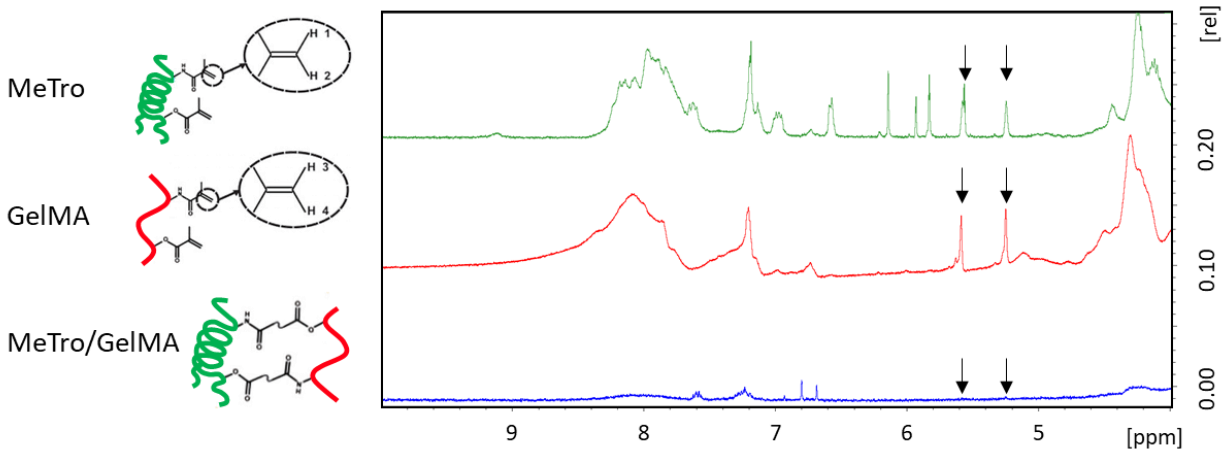

Figure S1. ^{1}H NMR (400 MHz; D_2O) spectra of MeTro prepolymer, GelMA prepolymer, and MeTro/GelMA hydrogels confirming the degree of crosslinking in the composite to be 87.7 %.

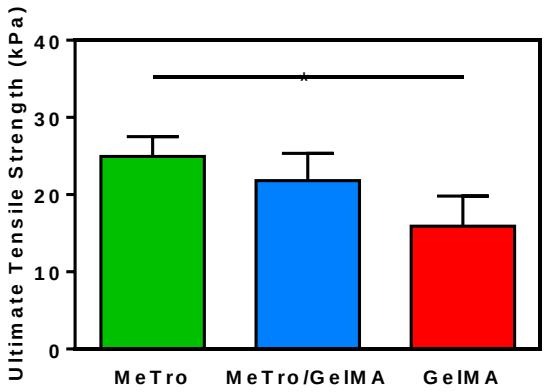

Figure S2. Ultimate tensile strength of MeTro, GelMA and MeTro/GelMA composite hydrogels. (* $p<0.05$)

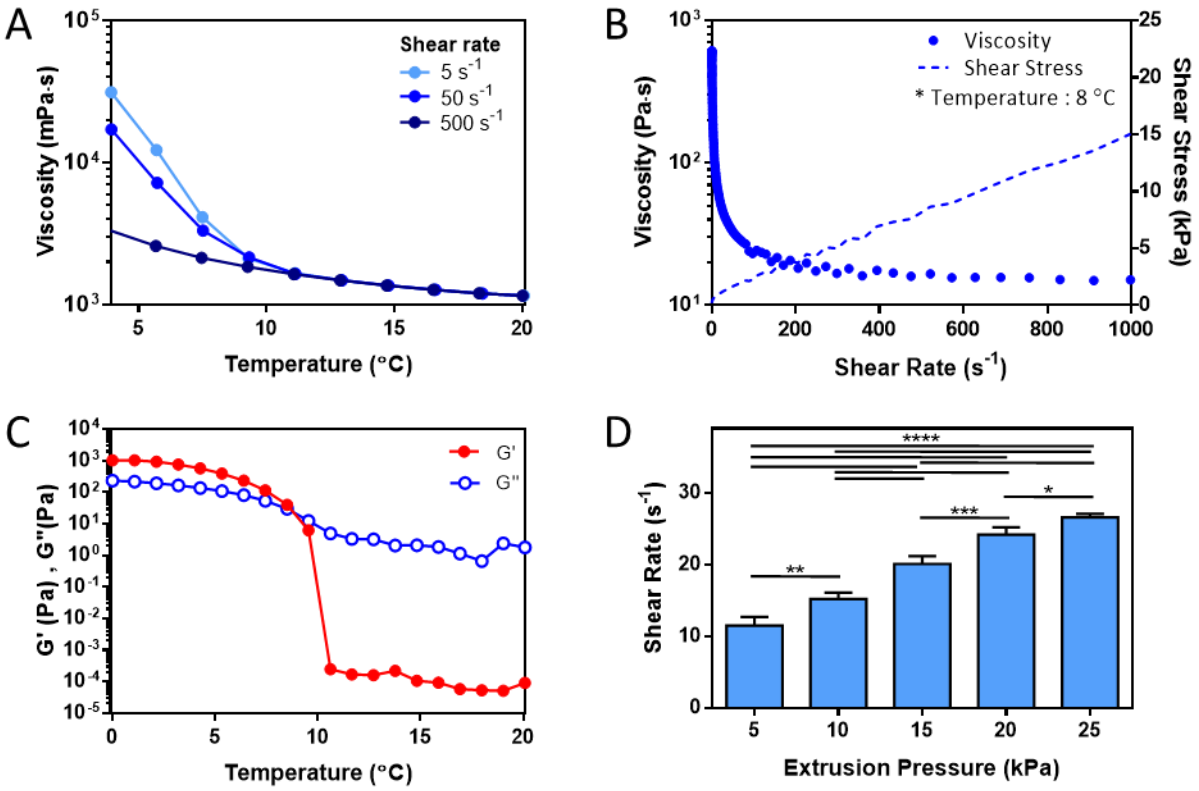

Figure S3. Rheological properties of MeTro/GelMA bioink. (A) Temperature dependence of viscosity of MeTro/GelMA bioink with different shear rate. (B) Viscosity and shear stress of MeTro/GelMA bioink as a function of shear rate. (C) Storage modulus, G′, and loss modulus, G″, of MeTro/GelMA bioink formulations as a function of temperature. (D) Shear rate during the 3D printing of MeTro/GelMA Bioink as a function of extrusion pressure. (* $p<0.05$, ** $p<0.01$, *** $p<0.001$, **** $p<0.0001$)

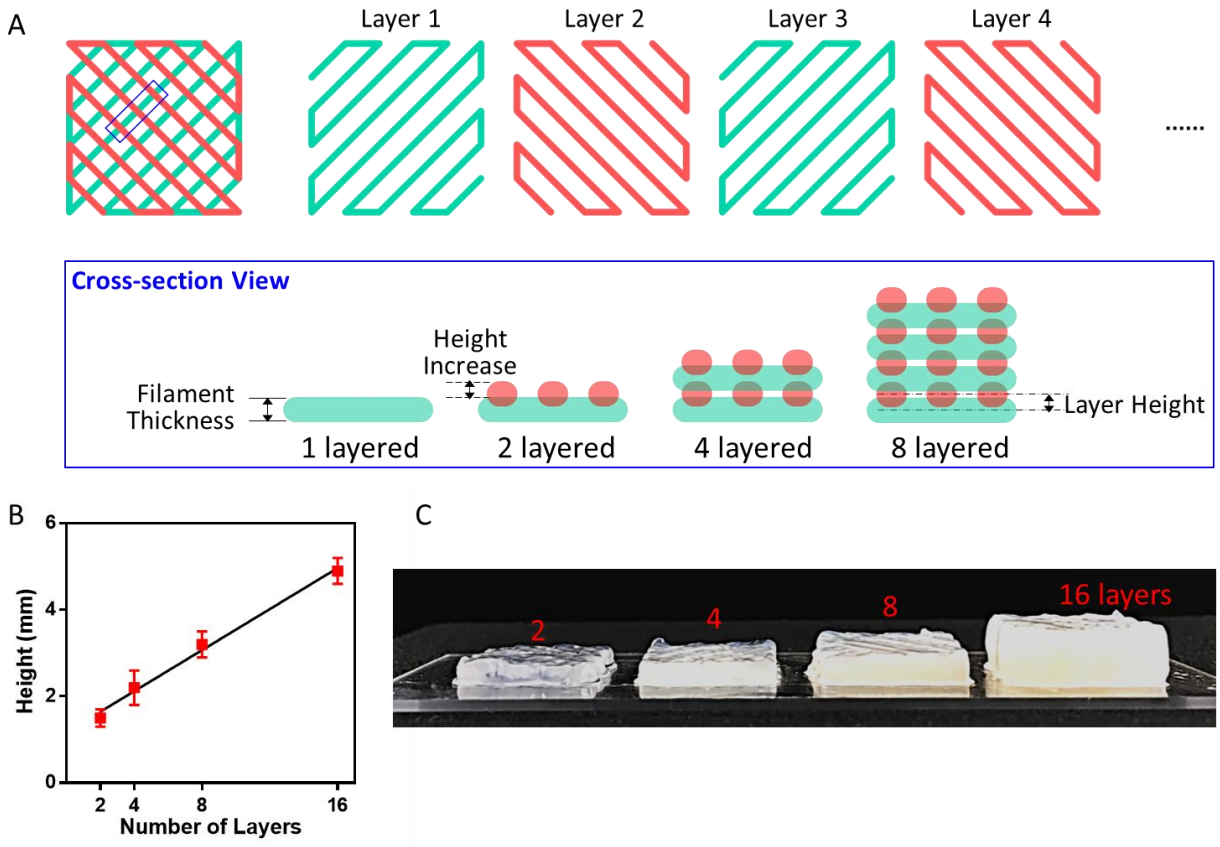

Figure S4. MeTro/GelMA lattice constructs printed up to 16 layers to form constructs with a linear relationship between the number of layers and the height. (A) Schematic representation of layer-by-layer printing of multi-layered lattice structure. Each layer was overlapped with the next layer to form an interconnected construct. (B) The heights of printed lattice constructs as a function of the number of layers. (C) Representative images of the printed lattice constructs with different number of layers.

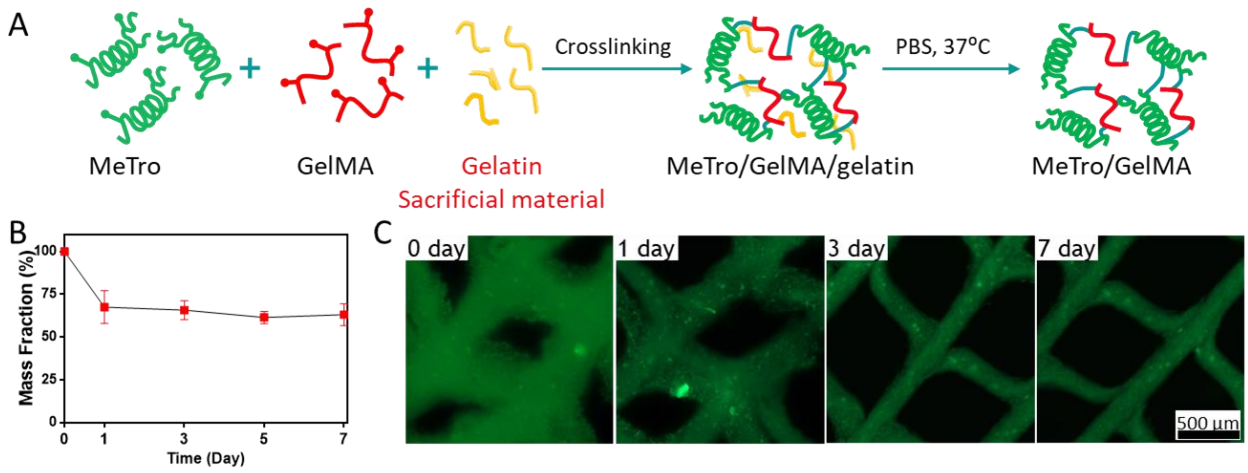

Figure S5. Post printing stability of 3D printed MeTro/GelMA constructs. (A) A Schematic illustration of gelatin diffusing out of the printed constructs during the incubation at 37 °C following the crosslinking. (B) Mass fraction of printed MeTro/GelMA constructs at days 0, 1, 3, 5 and 7 post incubation showing removal of remaining Carbopol and gelatin from the printed construct. (C) Microscope images of printed MeTro/GelMA constructs at days 0, 1, 3 and 7 post incubation.

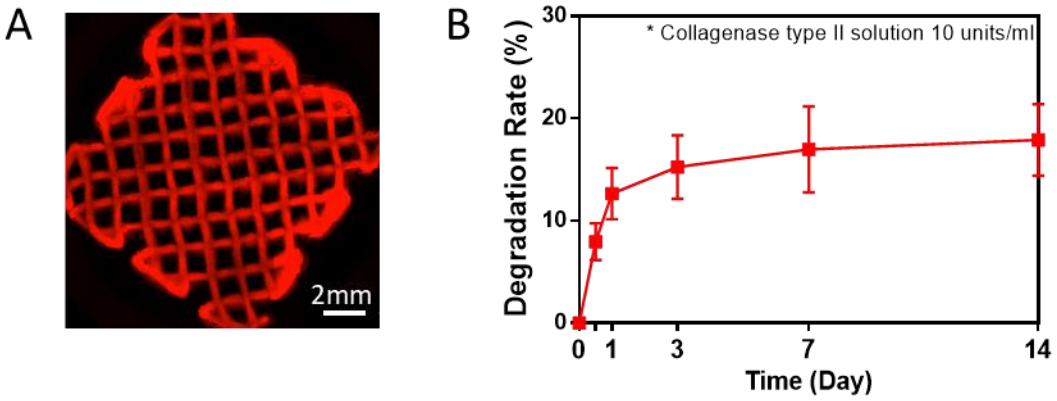

Figure S6. Degradation of the 3D construct. (A) A representative image of a lattice construct printed with MeTro/GelMA bioink for degradation test. (B) Degradation rate of the lattice construct at days 0.5, 1, 3, 7 and 14 post incubation in collagenase solution.

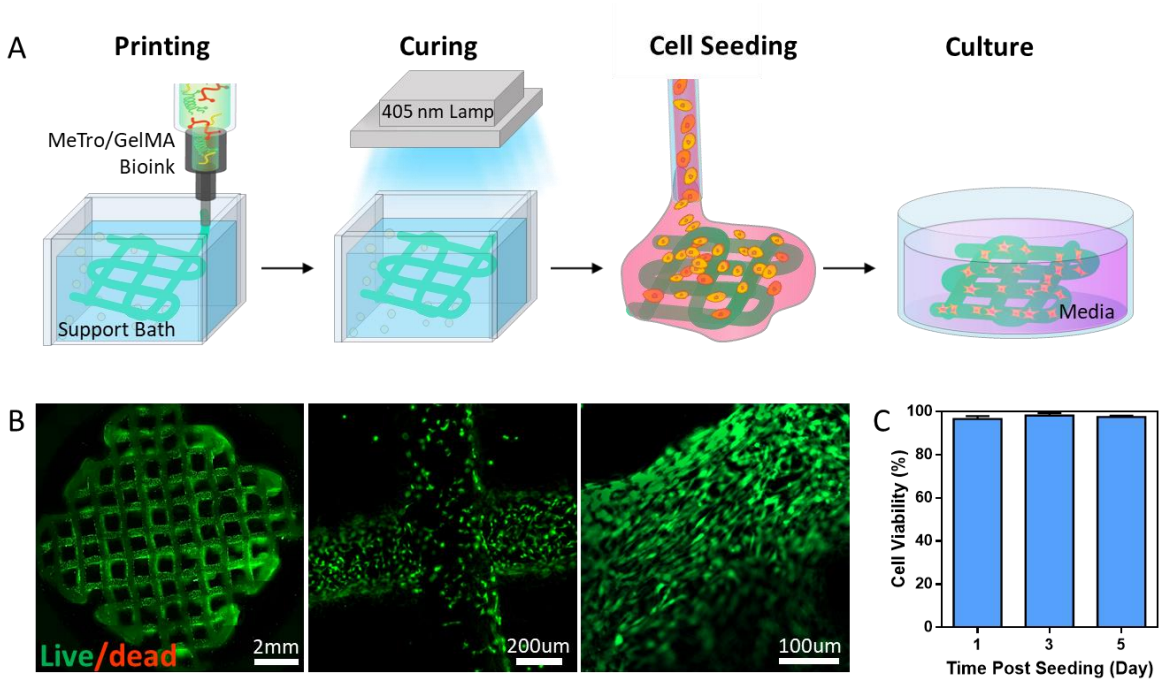

Figure S7. 2D cell seeding on 3D printed MeTro/GelMA constructs. (A) A schematic diagram of 2D cell seeding following the 3D bioprinting process. (B) Representative live/dead images of 3T3 cells seeded on 3D printed MeTro/GelMA constructs at day 3 post seeding. (C) Quantification of cell viability of 3T3 cells seeded on 3D printed MeTro/GelMA constructs at days 1, 3 and 5 post seeding.

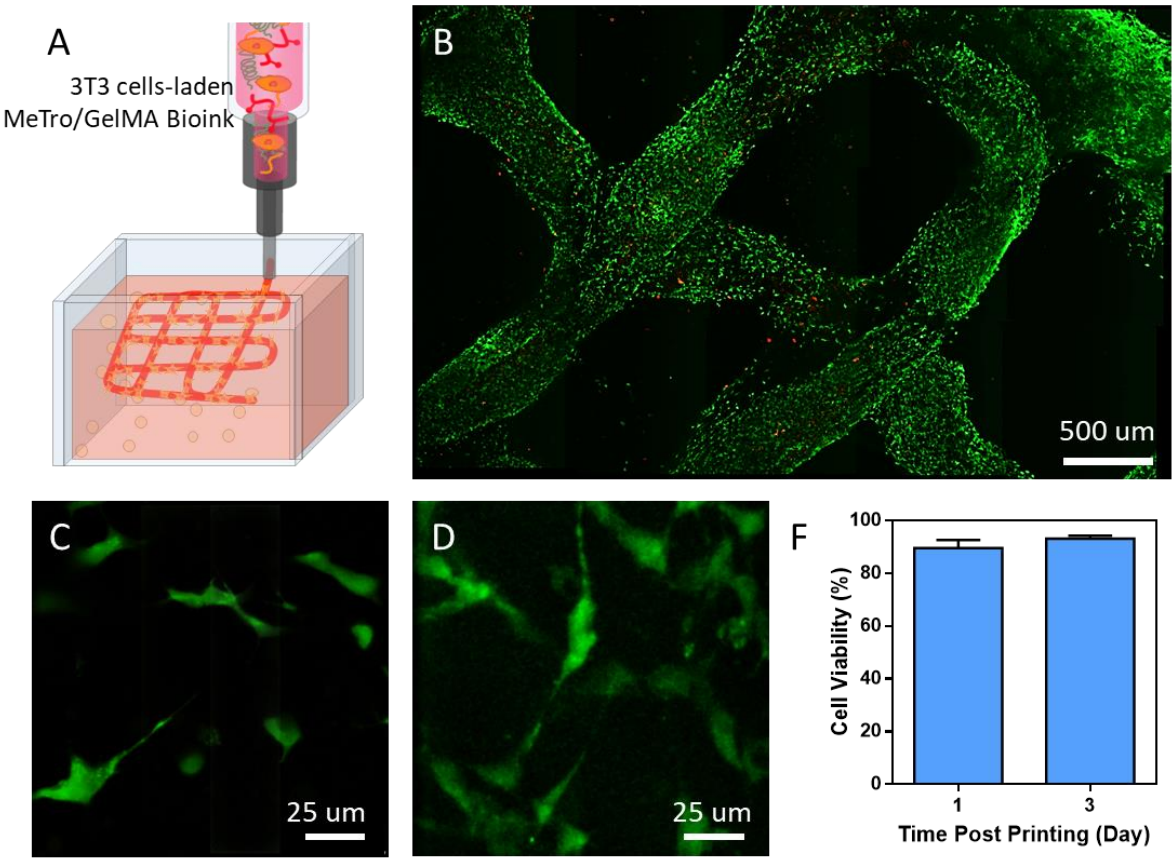

Figure S8. 3D bioprinting of 3T3 cell-laden MeTro/GelMA lattice. (A) Schematic showing the bioprinting of 3T3 cells-laden MeTro/GelMA bioink procedure. (B) A representative image of live/dead stained 3T3 cells within the 3D bioprinted MeTro/GelMA lattice at day 3. Representative live/dead images showing the distribution and spreading of 3T3 cells in the 3D bioprinted MeTro/GelMA constructs (C) at day 1 and (D) day 3 post printing. (C) Quantification of cell viability of 3T3 cells within 3D bioprinted MeTro/GelMA constructs at days 1 and 3 post bioprinting.

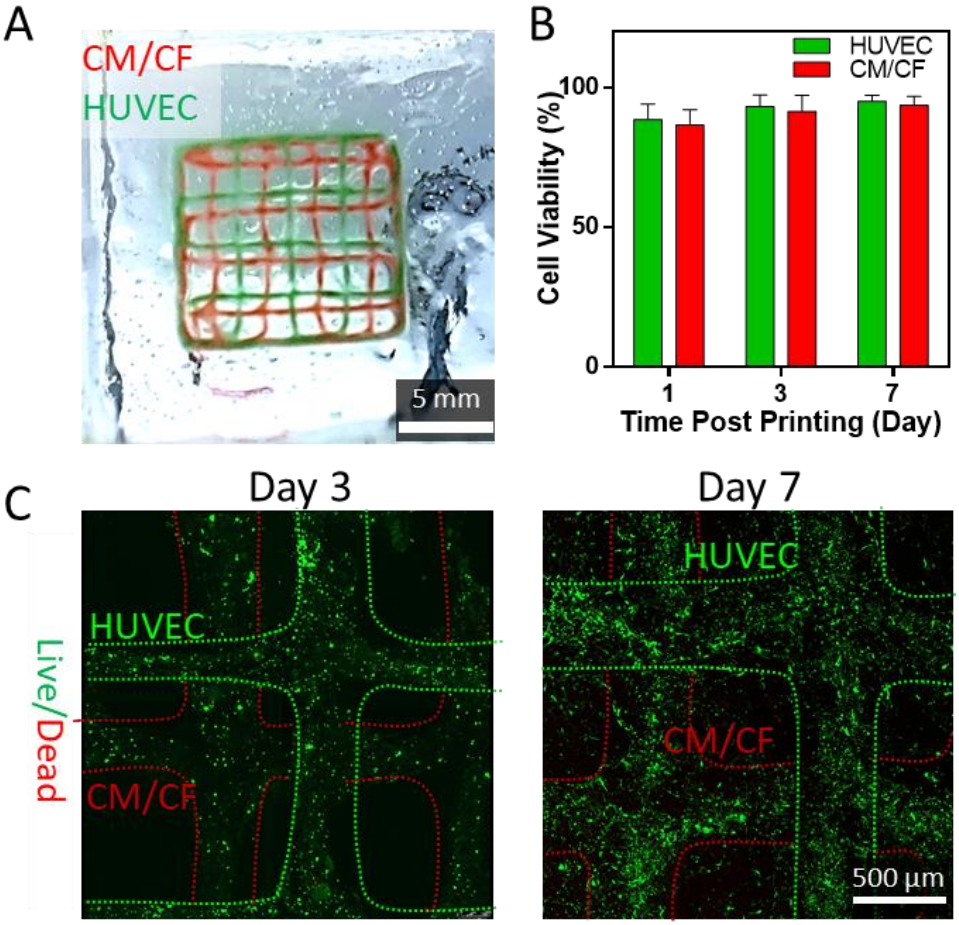

Figure S9. 3D bioprinting of lattice scaffolds containing HUVECs and CMs/CFs. (A) A representative image of the 3D printed lattice construct in the support bath. (B) Quantification of cell viability for 3D bioprinted cell-laden Metro/GelMA hydrogels at days 1, 3 and 7 post bioprinting. (C) Representative images of live/dead stained CMs/CFs and HUVECs incorporated within the construct at days 3 and 7 post bioprinting.

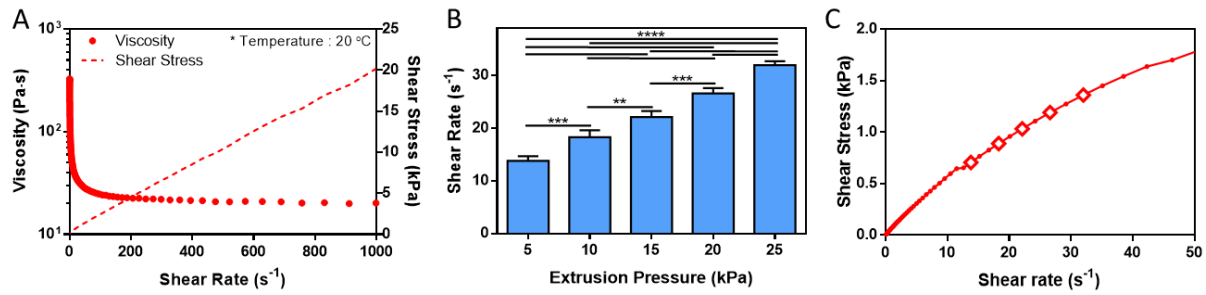

Figure S10. Rheological properties of GelMA bioink. (A) Viscosity and shear stress of GelMA bioink as a function of shear rate. (B) Varied shear rates of GelMA bioink depending on extrusion pressure. (C) Shear stress of GelMA bioink measured as a function of shear rate. The diamond points indicate the actual shear stresses on the cells encapsulated in the bioink exiting the nozzle under the extrusion pressures 5, 10, 15, 20, and 25 kPa, respectively (from left to right). (* $p<0.05$, ** $p<0.01$, *** $p<0.001$, **** $p<0.0001$)

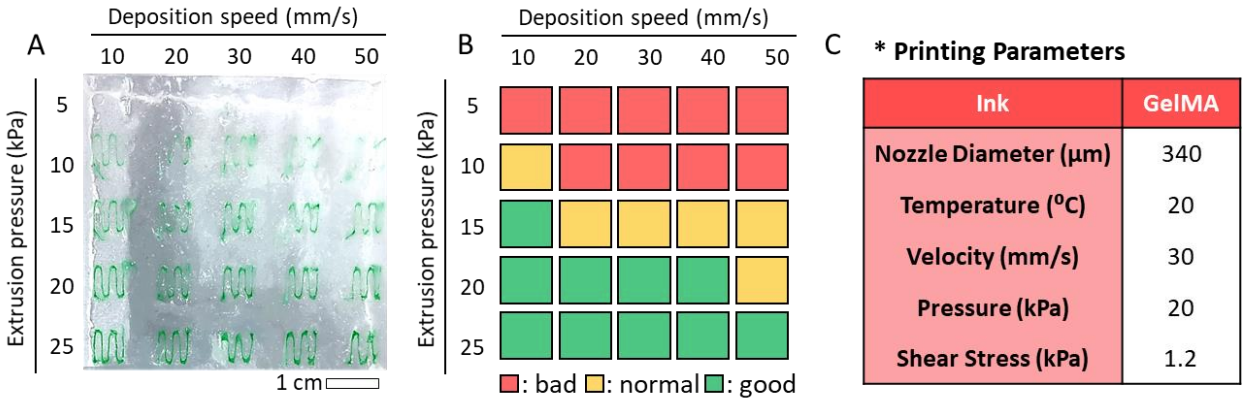

Figure S11. Optimization of printing conditions for GelMA bioink. (A) GelMA bioink filaments embedded into support bath with different printing pressures and speed. (B) Evaluation of printability of GelMA bioink with different printing pressures and speeds. (C) Optimized printing conditions for GelMA bioink.

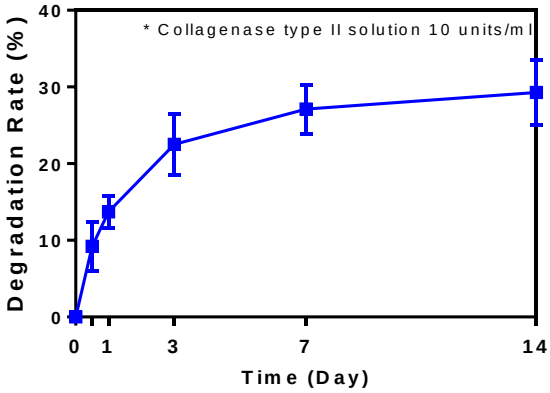

Figure S12. Degradation rate of lattice constructs printed with GelMA bioink at days 0.5, 1, 3, 7 and 14 post incubation in collagenase solution.

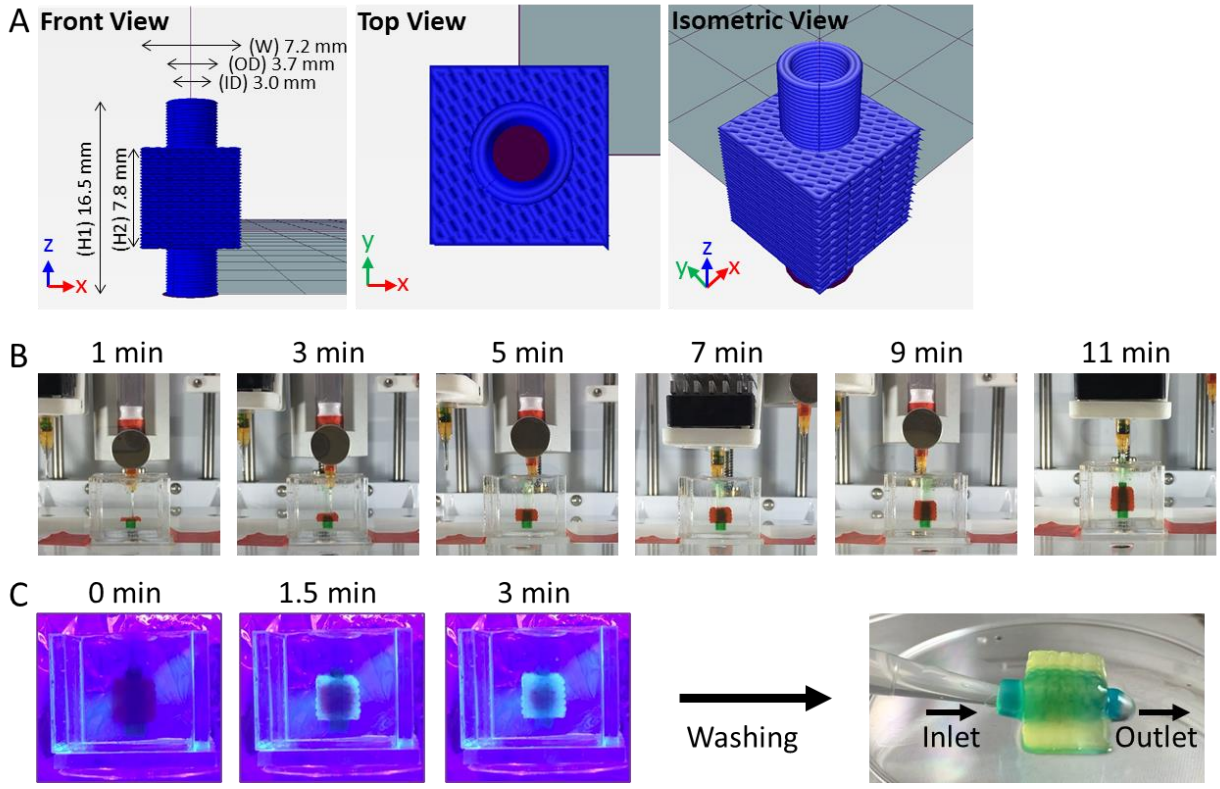

Figure S13. Representative images of 3D printed vascularized cardiac tissue model. (A) Schematic of the printed tissue model in different angles. (B) The process for 3D printing of the vascularized cardiac tissue construct. (C) Photocrosslinking of the printed construct with a 405 nm LED lamp. The printed structure was perfusable after washing step.

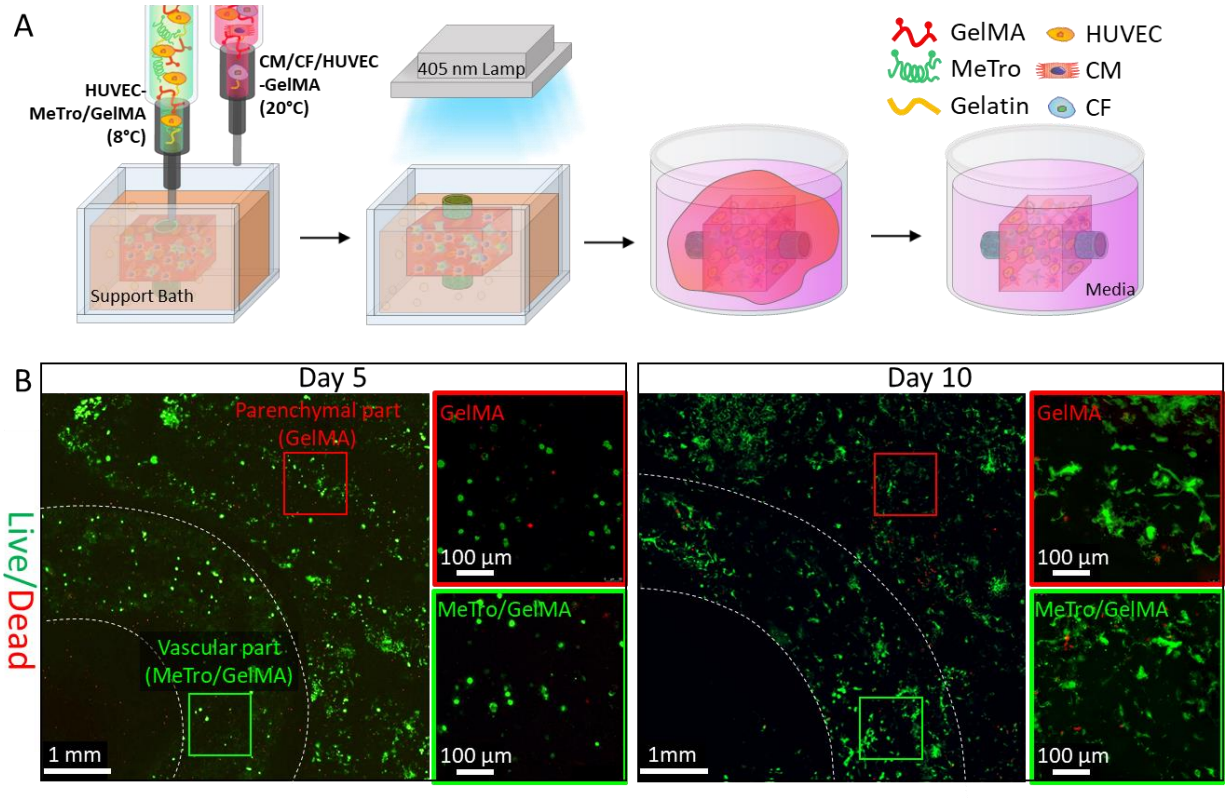

Figure S14. 3D bioprinting and live/dead staining of vascularized cardiac constructs. (A) A schematic illustration of 3D bioprinting vascularized cardiac constructs with HUVECs-laden MeTro/GelMA bioink and CMs/CFs/HUVECs-laden GelMA bioink. (B) Representative images of live/dead stained CMs, CFs and HUVECs incorporated within the bioprinted structure at days 5 and 10 post bioprinting. Parenchymal tissue printed with GelMA bioink and vasculature printed with MeTro/GelMA bioink are marked with red and green boxes, respectively.

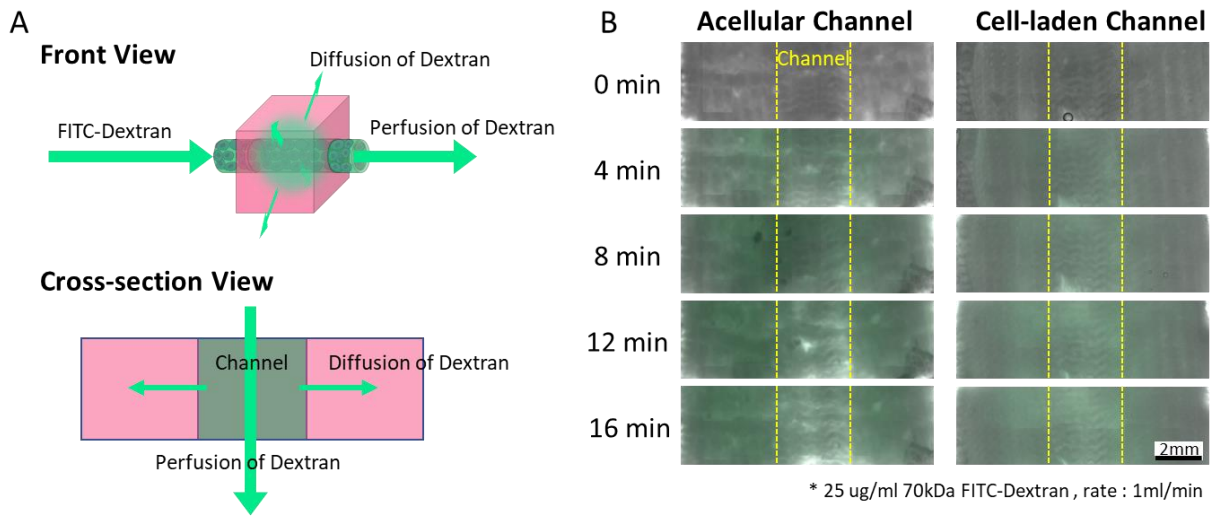

Figure S15. Evaluation of endothelium barrier function of 3D bioprinted constructs. (A) A schematic illustration of the barrier function test. (B) FITC-Dextran distribution within the constructs with acellular and HUVECs-laden channel 0, 4, 8, 12 and 16 min after infusion of FITC-Dex to quantify the barrier properties imparted by HUVECs in vascularized cardiac construct.

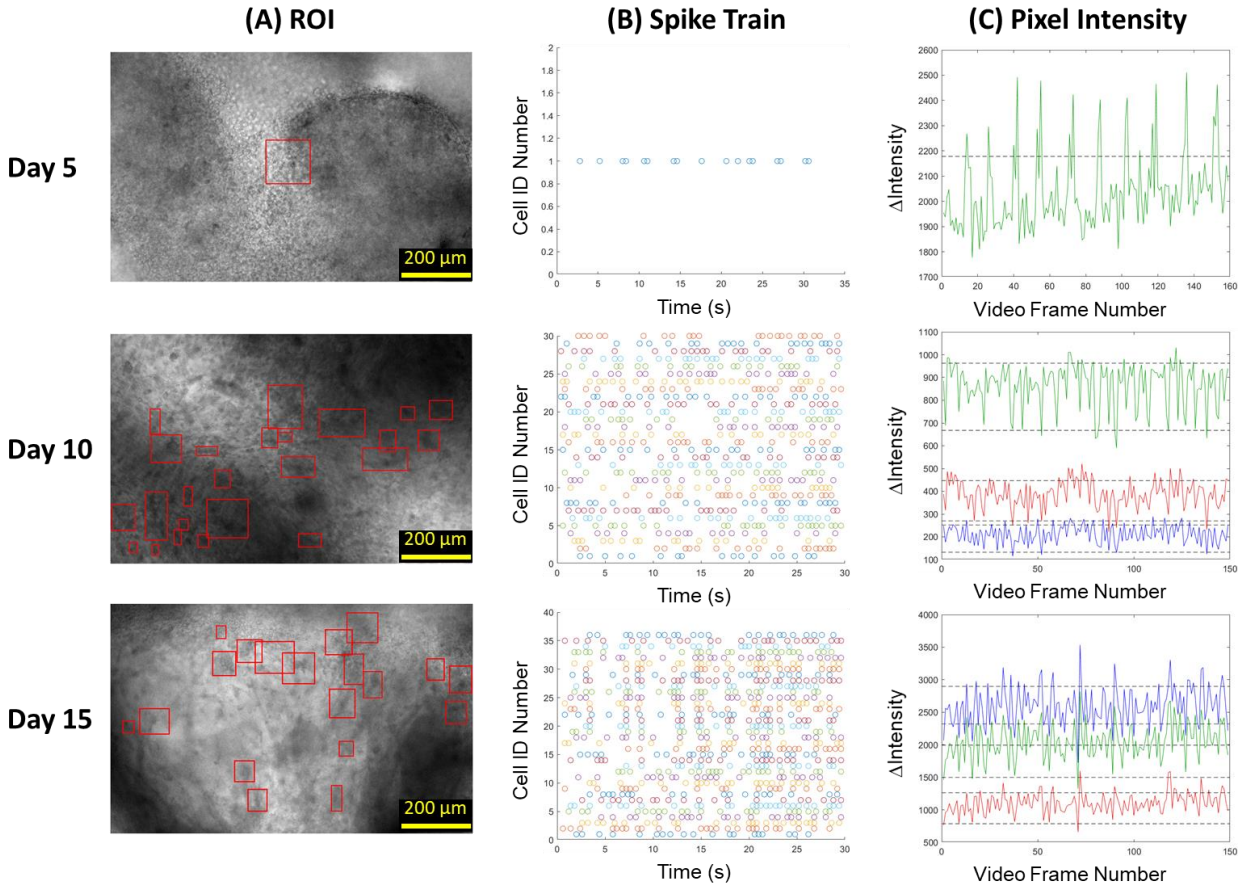

Figure S16. Evaluation of synchronized cardiac beating of 3D bioprinted constructs. (A) Representative bright field images with automated identification of encapsulated cells at day 5, 10 and 15 post bioprinting. (B) Representative spike train analogs used to quantify the degree of coordinated contractions of cardiac cells encapsulated in 3D bioprinted constructs at day 5, 10 and 15 post bioprinting. (C) Representative plots showing the change in pixel intensity over time for cardiac cells encapsulated in 3D bioprinted constructs at day 5, 10 and 15 post bioprinting.

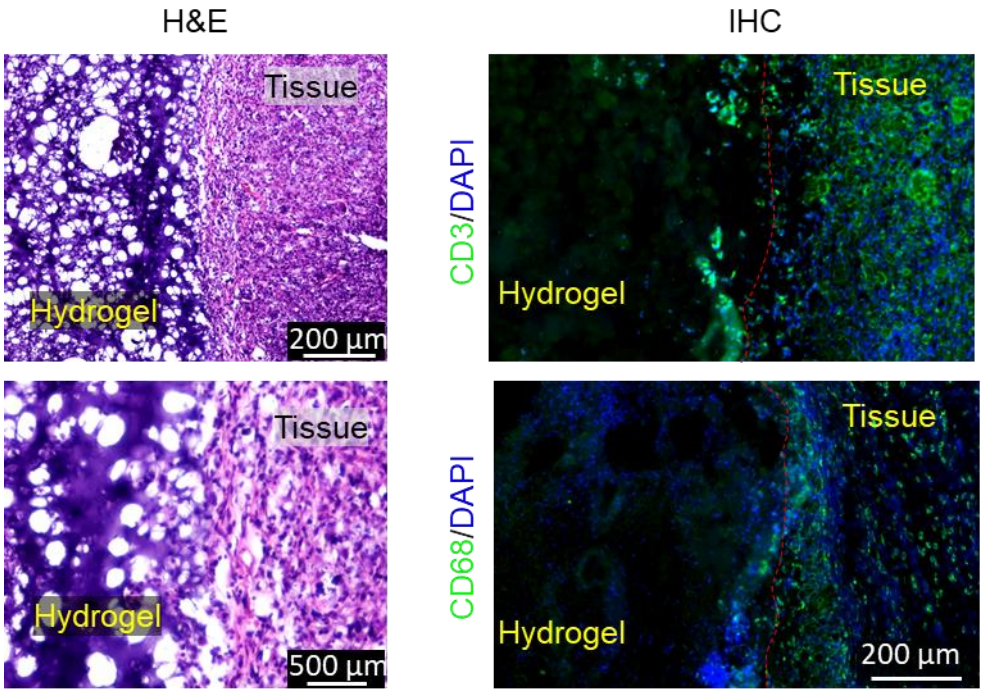

Figure S17. Representative H&E and IHC staining images of the subcutaneously implanted 3D printed and bioprinted cardiac constructs at day 14 post implantation.